Alwaha Sci. Publ. Services

Journal of Geomechanics and Geoengineering

Available at https://asps-journals.com

NF XP P94-424 standard shear test for estimating the mechanical properties of rock joints sampled from Yaounde gneisses (Cameroon)

Roger Bissaya [1]✉, Aurélie Kamwa Ngamy [2], Robert Eko Medjo [1], Richard Tanwi Ghogomu [1, 3], Bernard Njom [1]

1 *Department of Earth Sciences, University of Yaounde 1, Faculty of Science, Postal address: Box 812, Yaounde, Cameroon*

2 *Department of Mining Engineering and Treatment of Minerals, University of Maroua, Postal address: Box 46, Maroua, Cameroon*

3 *Department of Industrial Security, Quality and Environment, University of Maroua, Postal address: Box 46, Maroua, Cameroon*

Received August 23, 2021
Revised January 31, 2022
Accepted February 5, 2022
Published online: November 8,2022

Keywords
joint
rock mechanics
shear test
friction angle
Gneiss
Cameroon

Abstract: This study is a contribution to the knowledge of rocks mechanical properties in Yaounde, with a scope on failure parameters. In most instances, this goal is achieved by carrying out XP P94-424 standard shear tests. Thus, the tests were carried out on two joint samples, using the experimental device of the Fondasol laboratory (France). However, the pairs of shear – normal stress values were plotted or computed to determine other relevant parameters. The results are expressed as graphs and value reports. (1) The global friction angle β ranges around 36° for unsmoothed joints, and decreases up to 34° for smoothed joints. The friction angle ϕ ranges around 49° - 46° for unsmoothed joints, and decreases up to 3.90° for smoothed joints. The dilatancy i depend on the roughness and the type of joint surfaces; e. g. it ranged around 7° for the roughest surface while it ranged around 4° on the other. (2) At the peak the cohesion ranges around 81 kPa however, the wetness might affect this parameter up to its nullifying. At residual the cohesion ranges around 91 – 135 kPa.

1. Introduction

Hill slopes or excavated slopes have to cope permanently with the threat posed by landslides and rockfalls (Bell 1999; Cruden and Varnes 2006). These hazards result in the loss of lives, degradation and damage of infrastructure. When estimating the stability of slopes on surface and underground openings, pioneers (e. g., Hoek 1970; Jaeger 1972; Marachi et al. 1972; Barton 1973; Barton et al. 1974; Hoek and Bray 1977; 1981; Bieniawski 1976; 1978; Hoek and Brown 1980; 1997; Goodman 1980; 1989) have defined index values of mechanical parameter for soils and significant rocks specimen. All over the world experimental and theoretical research activities (e. g., Merrien-Soukatchoff and Gunzburger 2002; Manca 2006; Gasc-Barbier and Guittard 2009; Volkwein et al. 2011; Boccali et al. 2017; Guiheneuf et al. 2018; Wei et al. 2018) are addressed to the better understanding of the mechanical response of natural geomaterials. In Cameroon, research on this subject is new and focused on soils (e.g., Ekodeck 1990; 1994; Onana et al. 2007; Aboubakar et al. 2013; Mukenga et al. 2017). In Yaounde area, Mukenga et al. (2017) recently examined the evolution of soils mechanical parameters. Currently we are tracking in the same path for rock discontinuities. Here the mechanical parameters are usually obtained by laboratory tests, *in situ* tests being much more unusual for cost reasons. The presence or not of cemented infilling material can be a determining factor

✉ Corresponding author. E-mail address: rogerbissaya@gmail.com

in the mechanical behaviour of rock discontinuities. Assuming that the behaviour of discontinuities without infilling material depends only on the shape of the considered fracture surface, in the opposite case the behaviour depends on the infilling material. Usually the discontinuity may vary from unfilled to infilled during the same test. Simple shear test under normal constant stress allow both discontinuities to be characterized with the French standard XP P94-424 shear test (from AFNOR 2003). With this tool the aim of this work is to examine the discontinuity shear strength parameters characterizing the Yaounde gneisses as follows: (1) tangential steepness gradient; global friction angle and friction angle; geometric evolution, defined by dilatancy; and other relevant parameters (such as cohesion). (2) Then, the values suitability is discussed. The EN 1997-2 (2017) requirements for direct shear tests are fulfilled.

2. Geological setting

The study area geology is of the Yaounde group rocks comprising three distinct units (Champetier de Ribes and Aubagne 1956; Weeksteen 1957; Ball et al. 1984; Nzenti et al. 1988) (figure 1a-c). The metasedimentary unit is the more abundant; it includes paragneiss, some calco-silicate rocks and quartzites (Nzenti et al. 1988; Ngnotué et al. 2000; Mvondo et al., 2003). The metaplutonic unit comprises of orthogneiss (Nzenti et al. 1988; Ngnotué et al., 2000; Mvondo et al. 2003), amphibolites (Ngnotué et al. 2000) and pyroxenites (Nzenti, 1998). The micaschistous unit is comprised of recrystallized micaschist and quartzites (Champetier de Ribes and Aubagne 1957; Vicat 1998; Mvondo et al. 2003). These units possess tectonic features that are from the Pan-African thermo-tectonic event with several discontinuous structures. The D1 structures of the early Neoproterozoic correspond to shallowly incline exfoliation discontinuities sheet-like bands. The following D2 structures correspond to bidirectional stretching with boudins and vein joints that are of quartzo-feldspathic nature. The next D3 and D4 structures are of perpendicular contractions, accompanied by large exfoliated undulations. The late-Neoproterozoic brittle stage is characterized by unfiled and infilled steeply incline joints or fractures (Moreau and Ghogomu 1982; Mvondo et al. 2007; Mbola et al. 2014). Thus discontinuities that are likely to be or to generate failure are foliation and fracture planes. They should be accounted for appropriately in rock mechanics study as addressed in this paper.

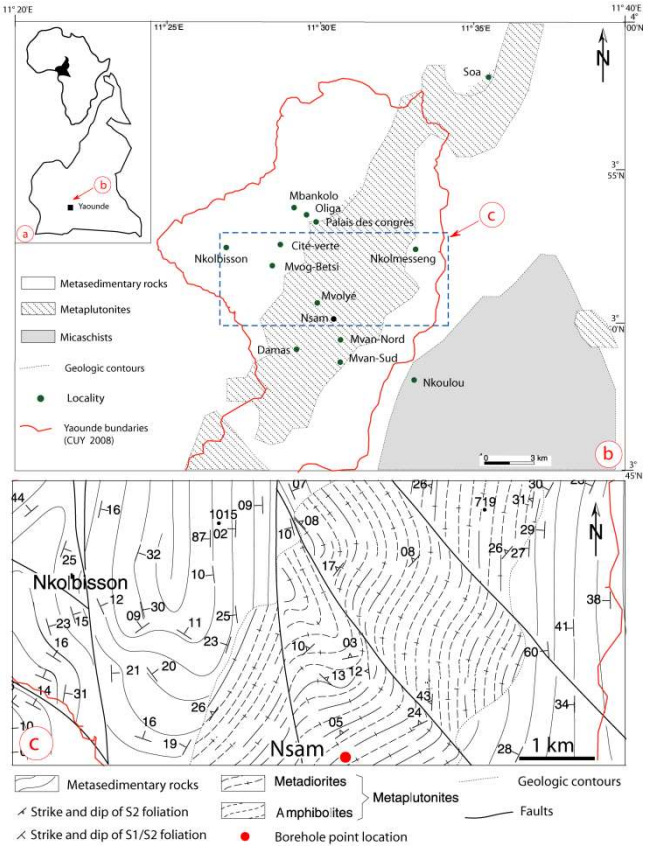

Fig. 1. (a) Location, (b) and extract of geological map of South Cameroon, (after Champetier de Ribes and Aubagne 1956; Weecksteen 1957). (c) Geological map of the borehole point surrounding area showing the main rock units and structures (modified from Mvondo and al. 2007).

3. Materials and methods

The direct shear test under normal constant stress or CNC (*Contrainte Normale Constante*) is described in the standard XP P94-424 (see Mazzoleni 1997; AFNOR 2003; AFTES 2003; ISRM 2007) (figure 2). The joint samples have been acquired by drilling core of 90 mm diameter. Their extractions from gneissic outcrop required geological and geotechnical experience and judgment to select a convenient borehole point location. Thus, Nsam quarry borehole point located N 03°49'09.9''and E 11°30'16.1'' has been chosen, according to the strike azimuth of 90°. From the acquired discontinuities, one was natural (joint sample 1) and the other was created through splitting (joint sample 2) (figures. 3a-d). Their discontinuity surfaces have been disposed in the mortar shells. The mortar shells have been sealed by potting material. Then the paralleled shells have been adjusted in the shear boxes of the shearing machine, and then blocked by tightening. Subsequently the specimens have been subjected under a constant normal stress σn while the tangential stress τ

increased until the relative movement of one epont. Therefore, the evolution of the tangential stress τ with respect to the relative displacement of the eponts (Ut; Un) could be measured. The standard XP P94-424 plans to do tests while applying at the same phase of shearing three values of normal stress. However, considering the insufficient length of the specimens for this operation, the tests were carried out with a first shearing, followed by a second and third shearing on the same surface; by applying respectively the highest stress (σn = 800 kPa), the medium stress (σn = 600 kPa), and the lowest stress (σn = 400 kPa). These decreasing second and third shearings are intended more for security purposes since on the solicited surface the breaking of epont asperities is already produced.

The rate of shearing adopted was 0.27 mm/min for every stage. The discontinuities were wetted in advance. Other relevant parameters were found by computing the peak resistance pairs of shear – normal stress values with the Mohr-Coulomb formula; and by plotting the maximum and final values of each stage within the reference (σn; τ). Here the Mohr-Coulomb strength model has been set up with the regression line, within Microsoft Excel program. The fitting of the regression line can be found in several Microsoft Excel tutorials (e. g., university of Pau internet site user guide*).

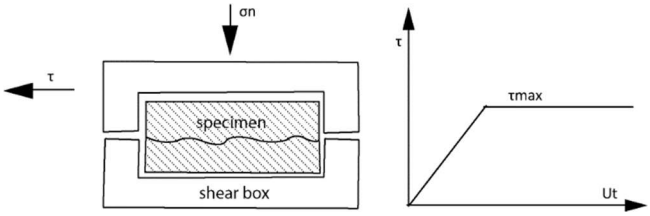

Fig. 2. Scheme of the applied direct shear test. (a) Cross section view, (b) shear stress vs. displacement curve (σn: normal stress, τ: shear stress, Ut: tangential displacement).

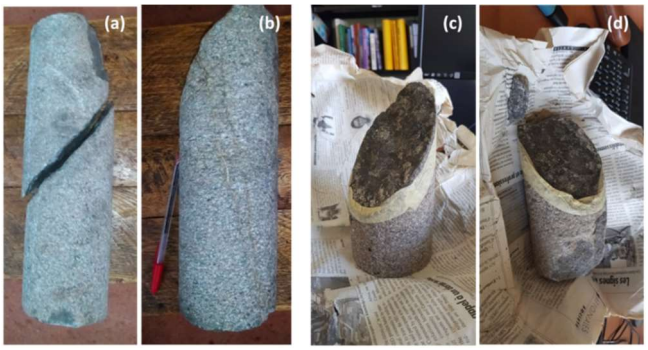

Fig. 3. Core segments of the discontinuities from (a) joint sample 1; (b) and joint sample 2. (c and d) Here the joint sample 1 discontinuity surfaces.

4. Results and discussions

4.1. Discontinuity characteristics

In this study the discontinuities designate fractures or cracks along which there are no displacements. From recovered cores, have been extracted sufficient discontinuities surfaces according to the scaling effect limit. Thus, the specimen 1 discontinuity was 46° dip angle (at 44° to core axis), whereas that of specimen 2 was 78°-80° dip angle (at 10°-12° to core axis). Their surface sizes were respectively 64.96 cm² and 49.27 cm² (figures. 4a-b).

4.2. Structure and petrography characteristics

The standard used is the ISO 14689-1 (Technical Committee ISO/TC 182 and Geotechnics Subcommittee SC 1, 2004), which is applicable to the rock description for geotechnical and engineering geology in the domain of civil engineering. It deals with the denomination, the description and the classification of rock materials and rock masses based on the mineral composition, the genetic aspects, the structure, the grain sizes and other parameters. Therefore the analysis has been carried out in macroscopic and microscopic scales. The macroscopic analysis has been made with the naked eye and the hand lens, *in situ* on the rock outcrop, and from the recovered sample. The microscopic analysis has been made with the aid of a microscope, using thin section. We have selected several scanned view according to the configuration of the microscope that was used (Ø =1.5 mm), and we have made an enlargement which is fifty times the real size (x50). The rock that is studied is of granulite facies gneiss. It is an intrusion rock in the area. With the naked eye, the rock has a grey colour, with compact habits, but without layers (figures 5a-b). Quartz constitutes 10 to 15% of its compound and its grains vary between 0.1 and 0.5 cm. Feldspars (orthoclase and plagioclase) constitute 15 to 20% of its composition and their size vary from 0.1 to 0.5 cm. Ferromagnetic minerals constitute 60 to 65% of its composition and their grains vary from 0.2 to 0.9 mm.

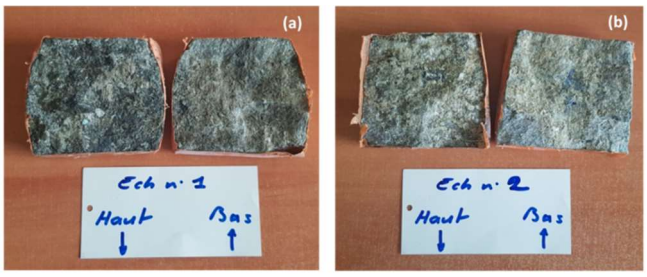

Fig. 4. Extracted discontinuity surfaces and their insertion in mortar shells; (a) specimen 1 and (b) specimen 2.

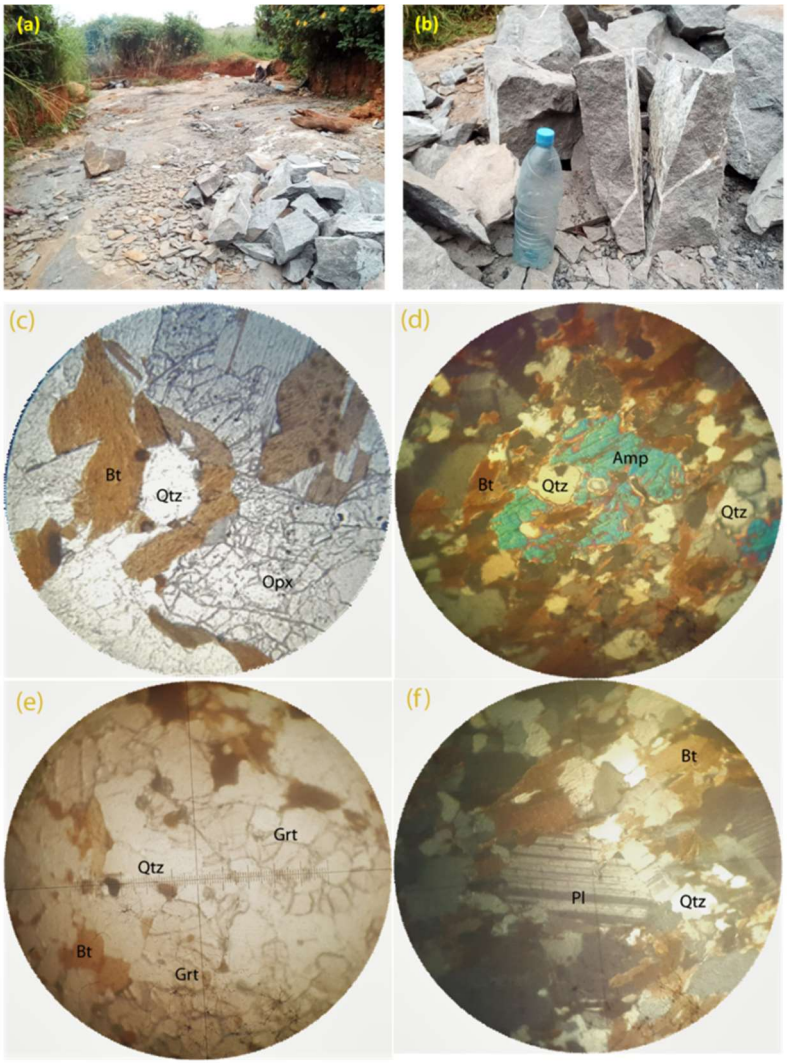

Fig. 5. Macroscopic and microscopic organization of sampled rock. (a and b) Sampling site at Nsam quarry (location N 03°49'36.0''; E 11°30'45,7''). The view of Ø =1.5 mm have been scanned into (c and e) plane-polarized light and (d and f) cross-polarized light. (Qtz: quartz, Pl: plagioclase, Bt: biotite, Grt: garnet, Mu: muscovite, Amp: amphibole, Opx: orthopyroxene). Note: bottle in figure b is 30 cm long.

Muscovite is in the form of very fine straws from 0.2 to 0.7 mm and it constitutes 2 to 5% of its composition. The rock is spotted with deep red coloured grains of garnet, their size vary from 0.1 to 0.2 cm and this garnet constitutes 10 to 20% of the rock composition. The other rock minerals are biotite, amphibole, pyroxene and opaque minerals such as graphite, rutile, zircon and monazite that are accessory. The rock thus presents pyroxene-rich and amphibole-rich clusters; which correspond respectively to pyroxenite and amphibolite. In the microscope, the rock has heterogranular granoblastic texture with xenomorphic orthopyroxene phenocrystals; its more detailed mineralogical setting is as follows:

- Pyroxene (40-50%) is very abundant in the rock. It presents orthopyroxene xenomorphic crystals of variable sizes (0.2 x 0.5 to 0.4 x 1 mm). They enclose inclusions of opaque minerals and quartz. (figure 5d).
- Biotite (10%) presents two habits: some minerals are secondary and xenomorphic (0.3 x 0.1 to 0.8 x 0.4 mm) (figures 5c-f).
- Quartz (10%) appears in the form of xenomorphic crystals (0.3 x 0.2 mm), some quartz crystals come in garnet inclusions; or are associated to pyroxene and feldspar crystals (figures 5c-f).
- Amphibole (5%) is of green hornblende crystals. It appears as xenomorphic crystals with quartz inclusions and with opaque minerals (0.3 x 0.1 to 0.8 x 0.4 mm) (figure 5d).

- Garnet (5%) appears as xenomorphic to sub-automorphic crystals (0.5 x 0.3 mm) and/or are elongated (0.8 x 0.16 mm). Some crystals are covered with quartz inclusions. Garnet is associated to biotite, plagioclase and quartz crystals (figure 5e).
- Alkali Feldspars (5%) is of orthoclase and plagioclase. Plagioclase (4%) is represented by xenomorphic crystals; these crystals are dispersed in the rock and have dimension of around 0.4 mm long. (figure 5f).
- Opaque minerals (2%) are inclusions in biotite, pyroxene and orthoclase.

4.3. Parameters characterizing the mechanical behaviour

4.3.1. Elasticity parameter defined by tangential steepness

The elasticity appeared when the specimens have been compressed initially to the higher value (800 kPa). At small displacement, the specimens behave elastically and the shear stress increases linearly with the displacement. The elasticity parameter is represented by tangential steepness gradient Ks (Eq. 1) (figure 6).

$$Ks = \frac{\delta\tau}{\delta Us} \quad (1)$$

where τ is tangential stress and Us is displacement.

Ks = 68.8° for specimen 1 and Ks = 66.7° for specimen 2.

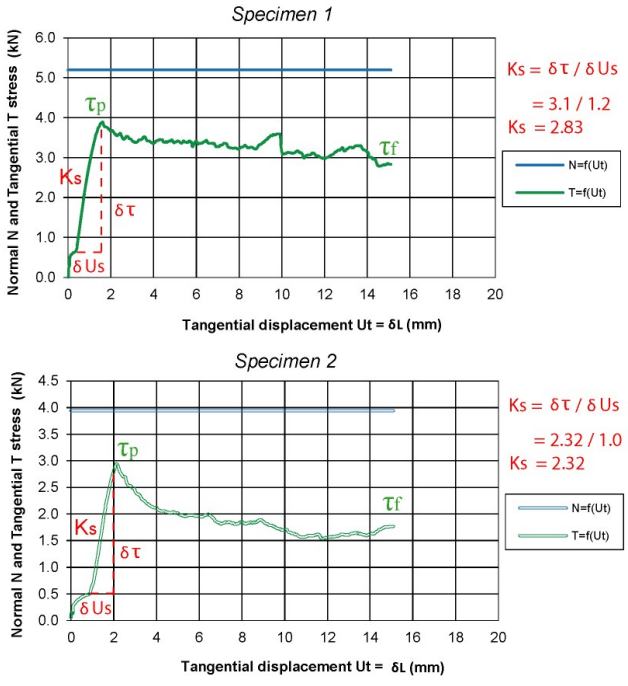

Fig. 6. Graphs of displacements showing high Ks gradient.

4.3.2. Variation of the shear resistance parameters defined by friction angle, dilatancy angle and global friction angle

In order to take account of changes in characteristics of the geometry of the surfaces, results of different tests are released in the form of graphs and value reports. Thus global friction angle β is function of the tangential displacement Ut (Eq. 2).The dilatancy angle i is function of tangential displacement Ut (Eq. 3). The friction angle ϕ which is function of tangential displacement is obtained from the measurement of β and i (Eq. 4).

$$\beta = \arctan\left(\frac{T}{N}\right) \quad (2)$$

where T is tangential effort and N is normal effort.

$$i = \arctan\left(\frac{\Delta Un}{\Delta Ut}\right) \quad (3)$$

where ΔUn is the variation of the normal displacement and ΔUt is the variation of the tangential displacement.

$$\beta = \varphi + i \quad (4)$$

The graphs can be interpreted as follows:

- For the first stage (figure 7) (σn = 800 kPa)

At the beginning of the tests dilatancy is 0° for both specimens; it then decreases to about -16° and then varies

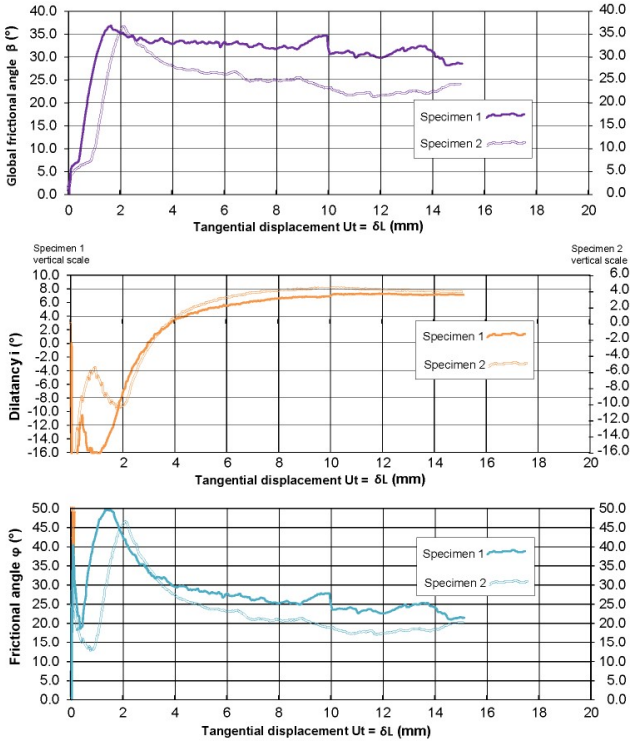

Fig. 7. Graphs of mechanical behaviour as function of tangential displacement in the first stage (σn = 800 kPa).

slightly between -10 and -6°; the geometry of the eponts is the cause of these variations because of the complete interlocking of the asperities. The friction angle reaches 40°, and then gradually increases to 50° in the first specimen and 46° in the second specimen. Finally, it gradually decreases respectively to 21° and 20°.

- For the second stage (figure 8) (σn = 600 kPa)

Note that the useful part of the graphs starts from 2 mm, when the dilatancy reaches the interlocking of the blunt asperities. The friction angle varies from 35° in the first specimen to 30° in the second specimen. Then it gradually increases to 30° and 25° respectively. Finally, it gradually decreases respectively to 25° and 22°.

- For the third stage (figure 9) (σn = 400 kPa)

Note that the useful part of the graphs starts from 2 mm, when the dilatancy reaches the interlocking of the blunt asperities. The friction angle varies from 46° in the first specimen to 37° in the second specimen at the beginning of the stage. Then it increases to 34° and 37° respectively. Finally, it gradually decreases to 30° and to 25°.

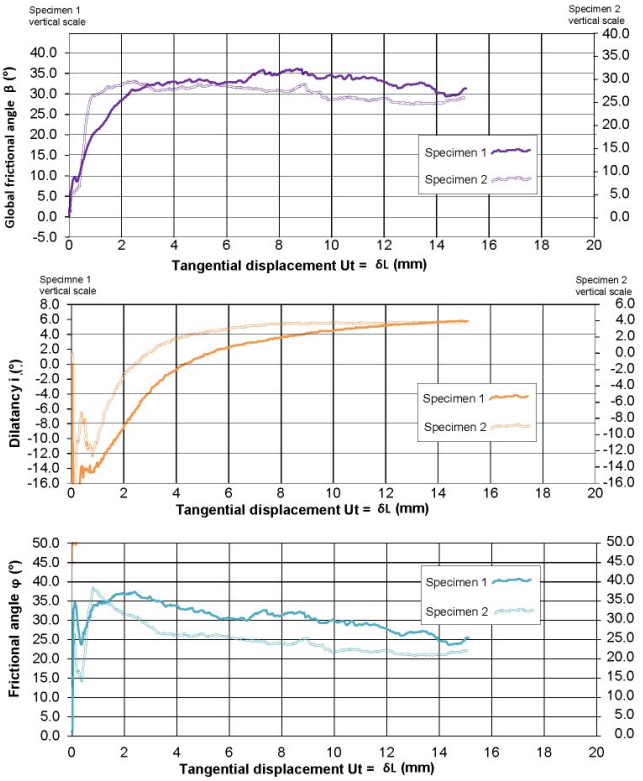

Fig. 8. Graphs of mechanical behaviour as function of tangential displacement in the second stage (σn = 600 kPa).

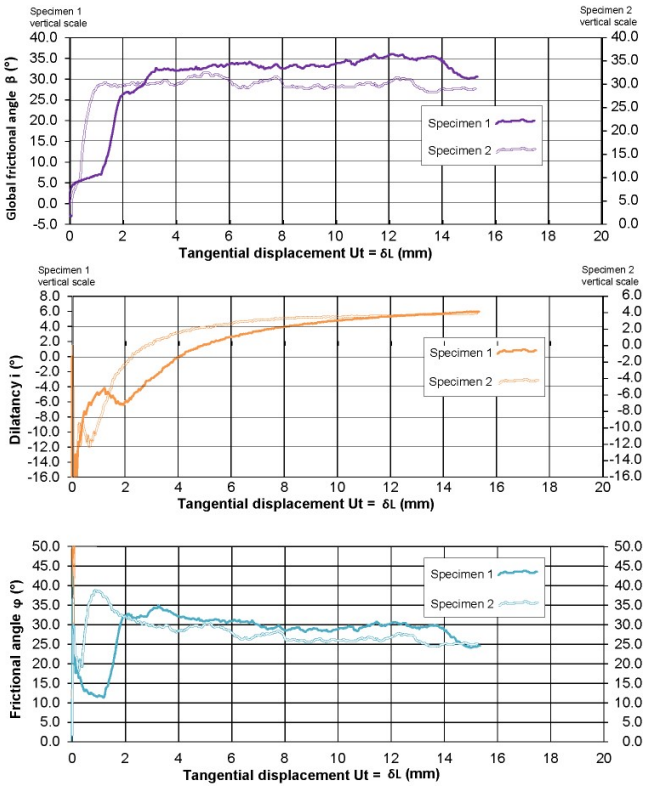

Fig. 9. Graphs of mechanical behaviour as function of tangential displacement in the third stage (σn = 400 kPa).

4.3.3. Geometric evolution parameter defined by dilatancy

The dilatancy is represented by a displacement of the eponts in the direction normal to the plane of the discontinuity. It is characterized by the dilatancy angle i (angle of the inclination of the dilatancy curve giving the normal displacement Un as a function of the tangential displacement Us). This angle has a maximum ip at the point of inflection of the dilatation curve. This point corresponds to the peak of the shear stress curve τ as a function of the tangential displacement Us, which represents, for the normal stress value (800 kPa), the rupture of the sharpest asperities. Beyond this value, the dilatancy continues at a lower angle defined by the more resistant asperities, with a wide base and low inclination; characterizing the very compact rocks such as gneisses (figure 10). Compared to clipped discontinuities, dilatancy induces an increase in peak resistance. According to the stages of testing undertaken, it has been a function of the alteration and interlocking of the eponts. The effect of abrasive (or filling) materials can also be seen in the constancy in dilatancy beyond the peak (figures 11, 12).

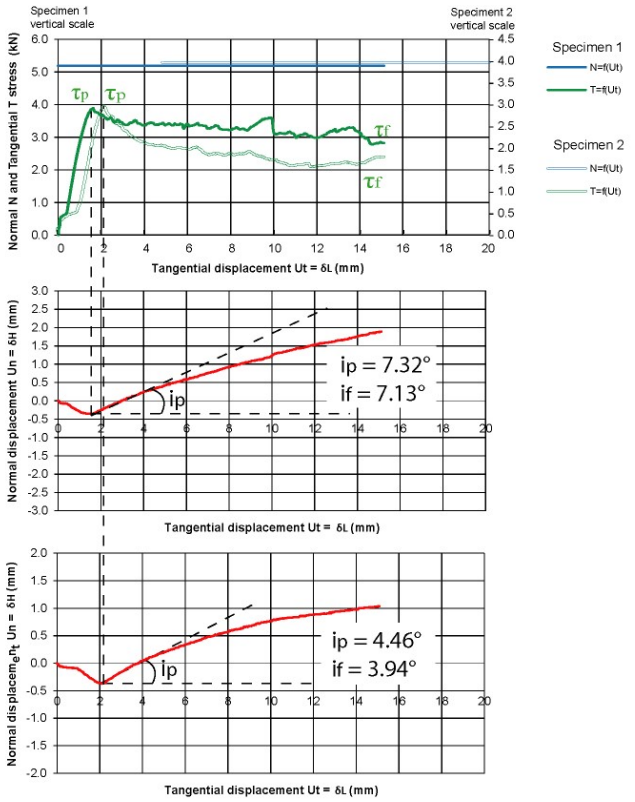

Fig. 10. Shear behaviour of the joint, highlighting the geometric response of the eponts in the first stage.

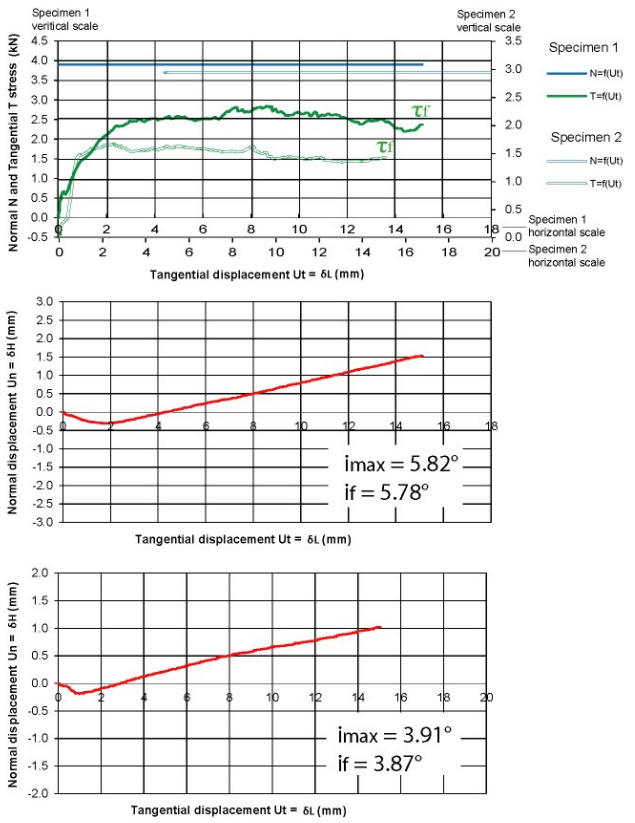

Fig. 11. Shear behaviour of the joint, highlighting the geometric response of the eponts in the second stage.

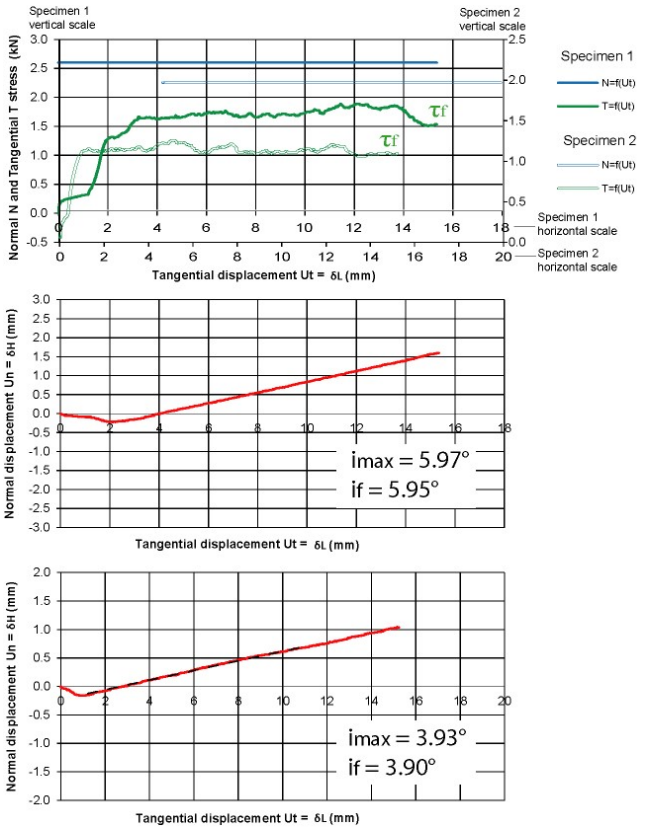

Fig. 12. Shear behaviour of the joint, highlighting the geometric response of the eponts in the third stage.

4.3.4. Values to be retained

Table 1 summarises what can be learned from the analyses at this stage. The peak shear strength parameters to be retained appear clearly. The peak global friction angle ranges around 36°. The friction angle ranges between 49°

Table 1. Failure parameters to be retained directly from lab data.

		Specimen 1			Specimen 2		
1st stage	σn (kPa)	β peak (°)	φ peak (°)	I (°)	β peak (°)	φ peak (°)	I (°)
	800	36.9	49.7	7.32	36.7	46.6	4.46
	σn (kPa)	β (°)	φ (°)	i (°)	β (°)	φ (°)	i (°)
	800	> 36.9 to 28.6	> 49.7 to 21.5	> 7.32 to 7.13	> 36.7 to 24.1	> 46.6 to 20.2	> 4.46 to 3.94
2nd stage	σn (kPa)	β (°)	φ (°)	i (°)	β (°)	φ (°)	i (°)
	600	36.1 to 31.3	37.4 to 25.4	5.82 to 5.78	29.71 to 26.06	38.27 to 22.18	3.91 to 3.87
3rd stage	σn (kPa)	β (°)	φ (°)	i (°)	β (°)	φ (°)	i (°)
	400	36 to 30.6	35 to 24.6	5.97 to 5.95	32.48 to 29.03	38.77 to 25.12	3.93 to 3.90

to 46°. The dilatncy depend on the roughness of the joint surfaces. It ranges around 7° for the specimen 1 (in the most undulated joint surface), and around 4° for the specimen 2 (in the least undulated joint surfaces). The residual strength parameters to be retained do not appear clearly at this stage. Thus, an extensive data processing of residual strength data is required. From the fit of the regression line, the Mohr-Coulomb criterion will be introduced.

4.4. Other failure parameters from further lab data analysis

4.4.1. Mohr-Coulomb computations and proposal of relevant parameters

Further exploitation of the shear stress data (see figure 13a-f) using the Mohr-Coulomb failure criterion allows other relevant parameters to be outlined. It is represented by the fitting linear envelope characterizing the peak strength and the residual strength; since both strengths are unequally sensitive to the scale effect. The additional parameters are peak cohesion, residual friction angle and residual cohesion.

The peak strength is a Coulomb's law performed by sample 1 and 2 equations (Eq. 3 and Eq. 4).

$$\tau peak = Cpeak + \sigma n \ tg\ 36.85° \quad (3)$$

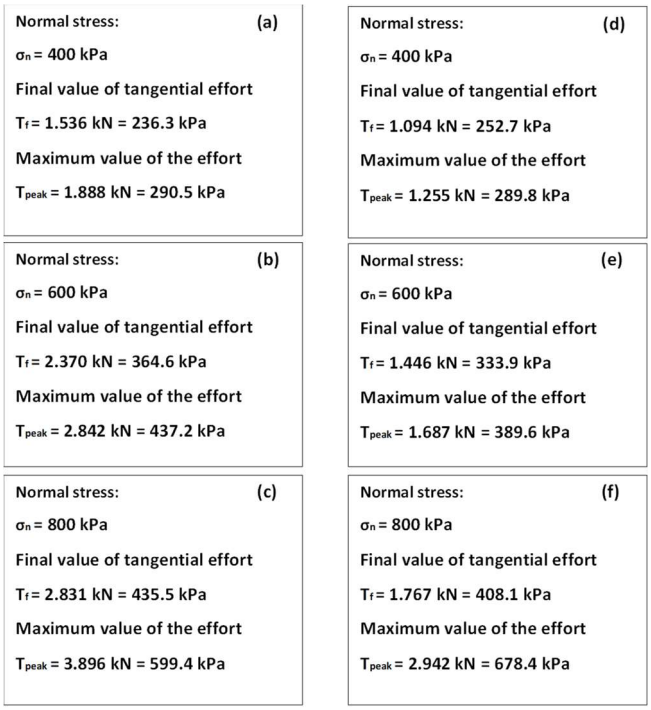

Fig. 13. Pairs of shear stress – normal stress values of (a, b, c) the specimen 1 and (d, e, f) the specimen 2 tests.

Table 2. Residual resistance values.

	Specimen 1		Specimen 2	
σn (kPa)	τmax (kPa)	τf (kPa)	τmax (kPa)	τf (kPa)
800		435.5		408.1
600	437.2		389.6	
600		364.6		333.9
400	290.5		289.8	
400		236.3		252.7

Table 3. Other relevant parameters from Mohr-Coulomb criterion.

	Peak values	Residual values
	Joint sample 1	
Cohesion (kPa)	-0.17 ≈ 0	91.3
Friction angle (°)		26.75
R^2		0.7741
	Joint sample 2	
Cohesion (kPa)	81.45	134.4
Friction angle (°)		20.50
R^2		0.8369

with τ_{peak} = 599.4 kPa and σn = 800 kPa.

$$\tau peak = Cpeak + \sigma n \ tg\ 36.73° \quad (4)$$

with τ_{peak} = 678.4 kPa and σn = 800 kPa.

The residual strength is a Coulomb's law performed by the regression line from residual resistance. From each stage σn and τ coordinates values (Table 2), the line-up of a straight line goes with the fitting of the regression line (figures 14a-b). Table 3 is a summary of the values found.

Why the peak failure parameters expressed by the Mohr-Coulomb criterion becomes of (Eq. 5) form in the specimen 1 data computation, since the cohesion is zero? Referring to the literature (e. g., Hoek and Bray 1981; Goodman 1989; Wyllie and Mah 2004) the zero cohesion from peak criteria is unusual. As presented above (see section 4.3.4), the dilatancy of the specimen under consideration at the peak is not very tight (ipeak = 7.32°). Moreover its discontinuity surface remained quite undulated up to the third test (if1 = 5.95° vs. if2 = 3.90°). Thus, the zero cohesion might come from wetness of the discontinuity.

$$\tau = \sigma n \ tg\ \varphi_{peak} \quad (5)$$

where τ is shear strength, σn is normal stress and ϕ is peak friction angle.

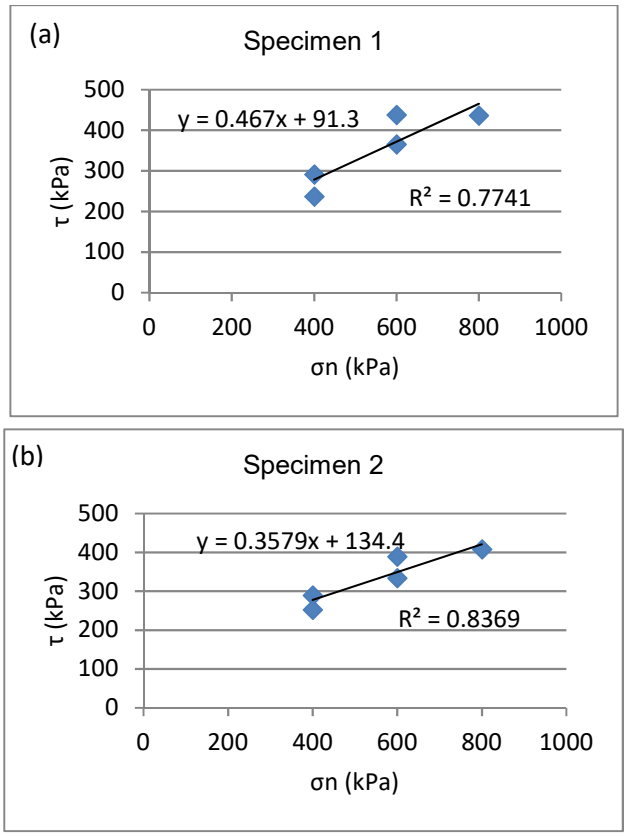

Fig. 14. Proposal of Mohr-Coulomb lines from (a) specimen 1 and (b) specimen 2 pairs of stresses values.

Might the residual data shear resistance express intrinsic material property? The cohesion may express an intrinsic material property of the eponts, however, since the joints are initially open; this refers to "apparent cohesion" (see Boncompain and Sauty 1975; Goodman 1989; Mazzoleni 1997; AFNOR 2003; Gasc-Barbier 2011), for it gives an approximate account of the roughness of the joint and the interlocking of the eponts. This property may also suggest the cohesive strength of the infilling material (see Wyllie and Mah 2004). In both cases the shear strength properties remain that of intrinsic material; i. e., although the discontinuities already contain an infilling for residual shear stress values, and the shear strength properties of the fractures are also modified, with both the cohesion and friction angle of the surfaces being influenced by the thickness and properties of the infilling (as shown in Tables 1 and 3), the rock and infilling are strong enough. Thus there is still important rock-to-rock contact, since thickness is not more than 25% of the amplitude of the asperities (after Goodman 1970).

4.4.2. About the errors calibration

The error value is a measure of how well a strength criterion fits a given data set. The Microsoft Excel calibration process minimizes the errors calibration. In fact, the correlation coefficients in our computation are R^2 = 0.7741 and R^2 = 0.8369. Assuming that when R^2 = 1, the fit of the Mohr-Coulomb line is perfect.

4.5. Relationship to some existing values

A comparison with the parameters of the Valabres gneisses (Table 4) shows light discrepancies with peak values and roughly equivalences with residual values. This may come from experimental conditions (e. g., wet vs. dry). Another comparison with rough surfaces from given sites (Table 5) and smooth surfaces such as the foliation planes of the graphitic schist from the Rennes region (figure 15) respectively suggests similarities with other type of gneisses, and reveals the effect of the lithology of the rock hosting the discontinuity through the decrease of the friction angle with the smoothness.

Table 4. Parameters of Valabres gneisses (after Gasc-Barbier 2011) versus that of the Yaounde area.

	Peak values	Residual values
Yaounde gneisses	Joint sample 1	
Cohesion (MPa)	0	0.913
Friction angle (°)	49.7	26.75
Yaounde gneisses	Joint sample 2	
Cohesion (MPa)	0.8145	0.1344
Friction angle (°)	46.59	20.50
Valabres gneisses		
Cohesion (MPa)	2.65	0.58
Friction angle (°)	25	20

Table 5. Failure parameters from given sites gneisses after Mazzoleni (1997) versus those of the Yaounde area.

		Sample 1 (Yaounde)	Sample 2 (Yaounde)	Sample 1 (given site)	Sample 2 (given site)
Rock type		Gneiss	Gneiss	Gneiss	Gneiss
Discontinuity type		Joint	Joint	Joint	Joint
Surface state		Rough	Rough	Rough	Rough
Surface size (cm²)		64.96	49.27	174	124
1st stage	σn (kPa)	800	800	610	630
	τp (kPa)	599.4	678.4	520	480
	φ (°)	49.7 - 21.5	46.6 - 20.2	29 - 32	22 - 26
	i (°)	7.32 - 7.13	5.97 - 5.95	11 - 7	12 - 6
2nd stage	σn (kPa)	600	600	390	490
	φ (°)	37.4 - 25.4	38.3 -22.2	35 - 37	25
	i (°)	5.82 - 5.78	3.91 - 3.87	7 - 6	7 - 5
3rd stage	σn (kPa)	400	400	200	280
	φ (°)	35 -24.63	38.8 - 25.1	37	25 - 27
	i (°)	5.97 - 5.95	3.93 - 3.90	6 - 4	5 - 0
	φr (°)	26.75	20.50	37	27

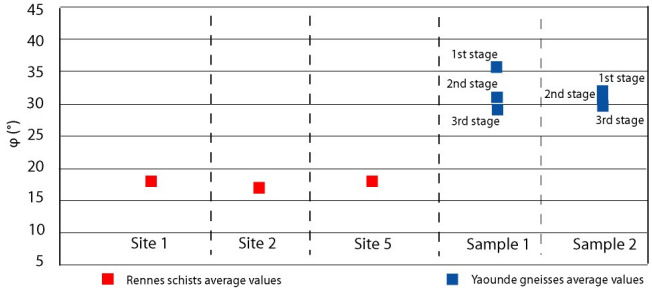

Fig. 15. Comparison to friction angles of the smooth joints of graphitic schists from Rennes region (after Guiheneuf et al. 2018, using the method developed by Le Cor et al. 2014).

4.6. Was there a downside to the application of new stress values on the same surface?

The calibration of experimental curves (anisotropic curve in green) to theoretical curves (isotropic curve in red and blue) shows a fairly good matching in the first stage, and the mismatch in the second and third stages (figure 16). In fact, behind the peak, there is a drop, approaching a parabolic shape in accordance with the model found in literature (e. g., AFNOR 2003; Mazzoleni 1997; Homand et al. 2001; Maksimovic 1996; 2002). Therefore, the use three times of the same discontinuity surface at progressively lower normal load did not affect the XP P94-424 shear test principle.

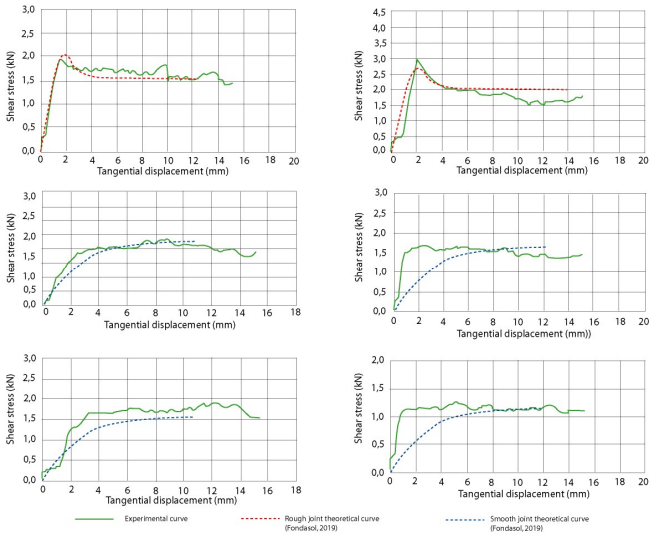

Fig. 16. Calibration of experimental curves to theoretical curves. Only the first stage curve (800 kPa) yield peak strength characteristics; the second (600 kPa) and the third (400 kPa) develop only residual type of resistance. Moreover, upper and bottom curves are more or less very close (shear stresses range around 1.5 kN). The theoretical curves (in red and blue) were outlined according to Fondasol (2019) lab tract.

5. Conclusion

This paper deals with the aim of extending the knowledge of rock mechanical properties in Cameroon. The results have been expressed as graphs and value reports, which made it possible to extract many relevant parameters. (1) The global friction angle β ranged around 36° for unsmoothed joints, and decreased up to 34° for smoothed joints. The friction angle ϕ ranged around 49° - 46° for unsmoothed joints, and decreased up to 3.90° for smoothed joints. The dilatancy i depended on the roughness and the type of joint surfaces; e. g. it ranged around 7° for the roughest surface while it ranged around 4° on the other. (2) At the peak the cohesion ranged around 81 kPa however, the wetness might have affected this parameter up to its nullifying. At residual, the cohesion ranged around 91 – 135 kPa. The stresses on the same surface did not affect the XP P 94-424 principle. The comparison of this study's results to that of other rocks parameter is secure, thus the use of this paper results in civil and geoengineering is prospective.

Acknowledgement

The authors are thankful to Eric PETITJEAN, Expert Geologist at the FONDASOL (France) geotechnical laboratory for carrying out the shear tests free of charge. The authors are thankful to the postgraduate research mate Jacques Bertrand ONANA who helped in the core sampling. The authors are thankful to anonymous reviewers for their insightful comments and suggestions. The authors are thankful to editor for assistance with helpful documents and additional suggestions.

Disclosures

Free Access to this article is sponsored by SARL ALPHA CRISTO INDUSTRIAL.

References

Aboubakar, B., Kagou, D.A, Nkouathio, D.G., Ngapgue, F. (2013) Instabilité de terrain dans les hautes terres de l'Ouest Cameroun : caractérisation géologique et géotechnique de glissement de terrain de kekem. Bulletin de l'Institut Scientifique, Rabat, Section Science de la Terre, 35: pp. 39-51.

AFNOR (Association Française de Normalisation) (2003) Cisaillement direct selon une discontinuité de roche – Essai sous un effort constant, normal à la surface de discontinuité. Norme XP P94-424, 12p.

AFTES (Association Française des Travaux Souterrains) (2003) Recommandations relatives à la caractérisation des massifs rocheux utiles à l'étude et à la realisation des ouvrages souterrains. Tunnels et ouvrages souterrains, n°177, 138-188.

Ball, E., Bard, J.P., Soba, D. (1984) Tectonique tangentielle dans la catazone panafricaine du Cameroun: les gneiss de Yaoundé. Journal of African Earth Sciences, 2: pp. 91-95.

Barton, N.R, Lien, R., Lundle, J. (1974) Engineering classification of rock masses for the design of tunnel support. Rock mechanics, 6: pp. 183-236.

Barton, N.R. (1973) Review of a new shear strength criterion for rock joints. Engineering Geology, Elsevier, 7: pp. 287-332.

Bell, G.F. (1999), Geological Hazards – Their assessment, avoidance and mitigation, E and FN Spon, London, 645p.

Bieniawski, Z.T. (1976) Rock mass classification in rock engineering. In: Exploration for rock engineering, Proc. Symp., Bri. Geotech; Soc. London, pp. 209-214.

Bieniawski, Z.T. (1978) Determinating rock mass deformability: Experience from case histories. Int. J. Rock Mech. Min. Sci. and Geomech. Abstr., 15: pp. 237-247.

Boccali, C., Biolchi, S., Zavagno, E., Zimi, L. (2017) Rock fall characterization in climbing spots: the case study of the "Napoleonica" Tourist Route (Trieste, NE Italy), In: Mikos, M., Tiwari, B., Yin, Y., Sassa, K. (eds), Advancing culture of living with landslides, 2, Springer, pp. 107-115.

Boncompain, B., Sauty, J.-P. (1976) Evaluation de la stabilité des pentes - Utilisation d'abaques - description et notice d'emploi du programme STABIL. BRGM, 75 SGN 332 AME, 59p.

Champetier de Ribes, G. and Aubagne, M. (1956) Notice explicative feuille Yaoundé Est. Avec carte de reconnaissance au 1/500000, Imprimerie Rébon, Paris.

Cruden, D.M., Varnes, D.J. (1986) Landslides types and processes, In: Turner, A.K., Schuster, R.L. (eds) Landslides: investigation and mitigation, Transportation Res. Board, Special Report 247, National Academy Press, Washington DC, pp. 36-75.

CUY (Communauté Urbaine de Yaoundé) (2008) Yaoundé 2020 – Plan directeur d'urbanisme. Rapport de présentation, 120p.

Ekodeck, G.E. (1990) Essai de corrélations entre paramètres altérologiques normatifs et caractères géotechniques des sols saturés : cas des produits d'altération des roches de la région de Yaoundé, Cameroun. Actes du Symposium International sur les sols structurés. AIGI, 9-13 avril, Yamoussoukro, Côte d'Ivoire, pp. 1-7.

Ekodeck, G.E. (1994) Un mode de caractérisation des sols résiduels compatibles avec les données de l'expérimentation géotechnique. Actes du 7e Congrès International de l'AIGI, Lisbonne (Portugal), pp. 3457-3468.

EN 1997-2 (2017) (English): Eurocode 7: Geotechnical design Part 2: Ground investigation and testing [Authority: the Europian Union Per Regulation 305/2011, Directive 98/34/EC, Directive 2004/18/EC], pp. 92.

Fondasol (2019) Essai de cisaillement roche, Présentation méthodologique. Prospectus du protocole de l'essai.

Gasc-Barbier, M. (2011) Comportement mécanique des roches: du laboratoire à l'ouvrage. Rapport de synthèse pour habilitation, Université Sciences et Technologies, Bordeaux.

Gasc-Barbier, M., Guittard, J. (2009) Comportement au cisaillement d'un joint rocheux naturel. Revue Française de Géotechnique, 128: pp. 5-13.

Ghiheneuf, S., Rangeard, D., Merrien-Soukatchoff, V., Dabard, M.-P. (2018) Caractérisation des plans de discontinuités des schistes du Briovrerien de la region de Rennes, Journées Nationales de Géotechniques et de Géologie de l'ingénieur, Champs-sur-Marne, 8p.

Goodman, R.E. (1970) The deformability of Joints. In determination of the in situ Modulus of Deformation of Rock. Am. Soc. Testing and Materials, Spec. Tech. Publication, No. 477, pp. 174-196.

Goodman, R.E. (1980) Introduction to rock mechanics, edited by John Wiley and Sons, New York.

Goodman, R.E., (1989) Introduction to rock mechanics, 2nd edition, John Wiley and Sons, 562p.

Hoek, E. (1970) Estimating the stability of excavated slopes in open-coast mines, Transactions Inst. Mining and Metallurgy, vol. 79, A109-A132.

Hoek, E., Bray, J. (1977) Rock Slope Engineering, 1st edition, IMM.

Hoek, E., Bray, J. (1981) Rock Slope Engineering, 3rd edition, Inst. Mining and Metallurgy, London, UK.

Hoek, E., Brown, E.T. (1997) Practical estimates or rock mass trength. Int. J. of Rock Mech. and Min. Sc. and Geomech. Abstr., 34(8): 1165-1186.

Homand, F., Belem, T., Souley, M. (2001) Friction and degradation of joints surfaces under shear loads. Int. J. Num. and Anal. Meth. in Geomech., 25: pp. 993-999.

ISRM (International Society of Rock Mechanics) (2007) The complete ISRM suggested methods for rock characterization, testing and monitoring – 1974-2006, Ulusay and Hudson (eds), Ankara, Turkey, 628p.

Jaeger, J.C. (1972) Rock mechanics and engineering, edited by Cambridge university press, London.

Le Cor, T., Rangeard, D., Merrien-Soukatchoff, V., Simon, J. (2014) Mechanical charactezation of weathered schists, 6: pp. 809-

812, Proceeding of 12th International NAEG Congress, Torino, Italy, 15-19 sept 2010.

Maksimovic, M. (1996) The shear strength components of a rough rock joint. International Journal of Rock Mechanics and Mining Sciences, Abst, 33 (8).

Maksimovic, M. (2002) A family of non-linear envelopes for non-cemented soils and rock discontinuities, Electronic Journal of Geotechnical Engineering.

Manca, P. (2006) Il progetto IFFI ed I resultati nella Regione Friuli Venezia Giulia. Atti del Congresso "I fenomeni franosi e gli strumenti per la loro mitigazione"

Marachi, N.D., Chan, C.K., Seed, H.B. (1972) Evaluation of properties of rockfill materials. J. Soil Mech. Fdns. Div. ASCE 98 (SM4), pp. 95-114.

Mazzoleni, G. (1997) L'essai de cisaillement de discontinuité rocheuse, Procédure et interprétation. Bulletin du laboratoire des ponts et chaussées, 211: pp. 89-99.

Mbola, N.S.P., Mvondo Ondoa, J., Owona, S., Nlongang, J.P.S., Olinga, B., Bilong, P. (2014) Evidence of the NE-SW extension in the Sa'a – Monatélé Region as in the Bafia and Yaounde Groups within the Central African Fold Belt (Cameroon): Implication for the Southern Cameroon Neoproterozoic extension. Sci., Tech. Dév., 15: pp. 1-15.

Merrien-Soukatchoff, V., Gunzburger, Y. (2002) Utilisation des classifications de massifs rocheux pour l'analyse du comportement de pentes. Présentation de deux cas d'application, Journées Nationales de Géotechniques et de Géologie de l'ingénieur, Nancy, 12p.

Moreau, M., Ghogomu, R.T. (1982) Résultats préliminaires à l'étude structurale des migmatites de Yaoundé. Annales de la Faculté des Sciences, Série IV, tome 1, pp. 105-111.

Mukenga, W., Havenith, H.-B., Medjo, E.R., Bissaya, R. (2017) Geotechnical assessment of potential mass movement occurrence in a zone at risk around Yaoundé-Cameroon. In: Mikos, M., Tiwari, B., Yin, Y., Sassa, K. (eds), Advancing culture of living with landslides, 2, Springer, pp. 455-463.

Mvondo, H., den Brok, S.W.J., Mvondo Ondoa, J. (2003) Evidence for symmetric extension and exhumation of the Yaounde nappe (Pan-African fold belt, Cameroon). Journal of African Earth Sciences, 36: pp. 215-231.

Mvondo, H., Owona, S., Mvondo Ondoa, J., Essono J. (2007), Tectonic evolution of the Yaounde segment of the Neoproterozoic Central African Orogenic Belt in southern Cameroon. Can. J. Earth Sci., 44: pp. 433-444.

Ngnotué, T., Nzenti, J.P., Barbey, P., Tchoua, F.M., (2000) The Ntui-Betamba high-grade gneisses: a northward extension of the Pan-African Yaoundé gneisses in Cameroon. Journal of African Earth Sciences, 31: pp. 369-381.

Nzenti, J.-P., Barbey, P., Macaudière, J., Soba D. (1988), Origin and evolution of the Late Precambrian high-grade Yaounde gneisses (Cameroon). Precambrian Research, 38: pp. 91-109.

Onana, V.L., Priso, E.N.E., Beyala, K.K., Ekodeck, G.E. (2007) Corrélation enre les paramètres altérologiques normatifs et les caractéristiques physico-méchaniques des roches de la série de Mbalmayo-Bengbis (Sud-Cameroun). 14e CRA MSG, Yaoundé, 26-28 Novembre 2007, pp. 155-164.

Technical Committee ISO/TC 182, Geotechnics Subcommittee SC 1. (2004) Geotechnical investigation and testing. Identification and classification of rock – Part 1: Identification and description, [https://geotechnicaldesign.info/iso14689-1-2003.html], last consulted on August 2020.

Vicat, J.P. (1998) Esquisse géologique du Cameroun. In: Vicat, J.P. et Bilong, P. (éds) Géosciences au Cameroun, Collection GEOCAM, Presses Universitaires de Yaoundé 1, 1: pp. 3-11.

Volkwein, A., Schelkenberg, K., Labiouse, V., Agliardi, F., Berger, F., Bourrier, F., Dorren, L.K.A., Gerber, W., Jaboyedoff, M. (2011) Rockfall characterization and structural protection - a review. Nat. Hazard Earth Sys., 11: pp. 2617-2651.

Weecksteen, G. (1957) Carte géologique de reconnaissance à l'échelle du 1:500 000, feuille Douala-Est avec notice explicative. Publication de la Direction des Mines et de la Géologie du Cameroun.

Wei, J., Liu, J., Song, Z., Zhu, Y., Bai, Y. (2018) Study on strength parameters of rock mass with stochastic combination discontinuities and their application in a tunnel in China. Advance in Mechanical Engineering, 10(7): pp. 1-21.

Wyllie, D.C., Mah, C.W. (2004) Rock Slope Engineering - Civil and Mining, 4th edition, Spon Press, 431p.

*University of Pau internet site user guide, https://www.iutbayonne.univ-pau.fr/~grau/1A/excel8.html). Consulted on the 19/01/2022.